Applied Physics Express

LETTER • **OPEN ACCESS**

Sub-pT magnetic field detection by tunnel magneto-resistive sensors

To cite this article: Mikihiko Oogane *et al* 2021 *Appl. Phys. Express* **14** 123002

OPEN ACCESS

Applied Physics Express 14, 123002 (2021) LETTER

https://doi.org/10.35848/1882-0786/ac3809

Sub-pT magnetic field detection by tunnel magneto-resistive sensors

Mikihiko Oogane[1,2,3*], Kosuke Fujiwara[4], Akitake Kanno[5], Takafumi Nakano[1], Hiroshi Wagatsuma[4], Tadashi Arimoto[6], Shigemi Mizukami[7,2,3], Seiji Kumagai[4], Hitoshi Matsuzaki[1,4], Nobukazu Nakasato[5], and Yasuo Ando[1,2,3]

[1]Department of Applied Physics, Graduate School of Engineering, Tohoku University, Sendai, Miyagi 980-8579, Japan
[2]Center for Science and Innovation in Spintronics (Core Research Cluster) Organization for Advanced Studies, Tohoku University, Sendai, Miyagi 980-8577, Japan
[3]Center for Spintronics Research Network, Tohoku University, Sendai, Miyagi 980-8577, Japan
[4]Spin Sensing Factory Corp., Sendai, Miyagi 980-8579, Japan
[5]Department of Epileptology, Tohoku University School of Medicine, Sendai, Miyagi 980-8575, Japan
[6]KONICA MINOLTA, INC., Tokyo 192-8505, Japan
[7]Advanced Institute for Materials Research, Tohoku University, Sendai Miyagi 980-8577, Japan

*E-mail: oogane@mlab.apph.tohoku.ac.jp

Received October 13, 2021; revised October 28, 2021; accepted November 9, 2021; published online November 22, 2021

We developed tunnel magneto-resistive (TMR) sensors based on magnetic tunnel junctions (MTJs) that are able to detect a weak, sub-pT, magnetic field at a low frequency. Small detectivities of 0.94 pT/Hz$^{1/2}$ at 1 Hz and 0.05 pT/Hz$^{1/2}$ at 1 kHz were achieved by lowering the resistance of MTJs and enhancement of the signal using a thick CoFeSiB layer and magnetic flux concentrators. We demonstrated real-time measurement of magnetocardiography (MCG) and nuclear magnetic resonance (NMR) of protons using developed sensors. This result shows that both MCG and NMR can be measured by the same measurement system with ultra-sensitive TMR sensors. © 2021 The Author(s). Published on behalf of The Japan Society of Applied Physics by IOP Publishing Ltd

A giant tunnel magnetoresistance (TMR) effect in magnetic tunnel junctions (MTJs) with Fe(001)/MgO(001)/Fe(001) structure was predicted by theoretical calculation.[1,2] This TMR effect is caused by the quantum coherent tunneling of electron spins through a MgO barrier layer. This revolutionary phenomenon was experimentally demonstrated in epitaxially grown Fe/MgO/Fe-MTJs fabricated using the molecular beam epitaxy method.[3] After the first demonstration of the giant TMR effect, S. Yuasa et al. and S. S. P. Parkin et al. reported a very large TMR ratio of about 200% at room temperature in MTJs with MgO barrier layers.[4,5] Furthermore, D. Djayaprawira et al. Fabricated MTJs with CoFeB/MgO/CoFeB structure on Si substrates and observed a huge TMR ratio of 230% at room temperature.[6] To date, the TMR ratio in CoFeB/MgO/CoFeB-MTJs at room temperature has improved to 600%.[7]

After the discovery of the giant TMR effect, research and development for applying MTJs to spintronic devices, such as the magnetic random-access memory and reading sensors for hard-disk drives, have been actively carried out.[8–10] Recently, MTJs based on the CoFeB/MgO/CoFeB structure with both high TMR and soft magnetic properties have been developed, and it is expected that they will be applied to highly sensitive magnetic sensors for detecting a weak magnetic field such as a bio-magnetic field.[11–14] Because of the dramatic increase in sensitivity of TMR sensors in recent years, the detection of the weak bio-magnetic field, such as cardiac magnetic field (magnetocardiography: MCG) and brain magnetic field (magnetoencephalography: MEG), have been demonstrated at room temperature with TMR sensors.[14] However, further improvement in the detectivity of TMR sensors is required to realize the TMR-based bio-magnetic field measurement system.

In this study, we have achieved the lowest magnetic field detectivity of 0.94 pT/Hz$^{1/2}$ at 1 Hz in the TMR sensor by improvement of the soft magnetic properties for the free layer, reducing the device resistance and using a magnetic flux concentrator (MFC) structure. By using the TMR sensor with low magnetic field detectivity at a low frequency, we observed clear MCG signals in real-time measurement. Further, the developed TMR sensor has an extremely low magnetic field detectivity of 0.05 pT/Hz$^{1/2}$ at 1 kHz. Protons in the human body generate nuclear magnetic resonance (NMR) at a frequency of 1–4 kHz under a weak magnetic field of 25–100 μT range, and we succeeded in measuring the NMR signal of protons for the first time using the TMR sensor.

MTJ multilayer films were deposited on thermally oxidized Si wafers using an ultra-high-vacuum ($P_{base} < 1 \times 10^{-6}$ Pa) sputtering system. The stacking structure was Sub. Si, SiO_2/bottom electrode/$Co_{70.5}Fe_{4.5}Si_{15}B_{10}$ 140/Ru 0.4/$Co_{40}Fe_{40}B_{20}$ 3/MgO/$Co_{40}Fe_{40}B_{20}$ 3/Ru 0.9/$Co_{75}Fe_{25}$ 2/$Ir_{22}Mn_{78}$ 10/Ta 5/Pt 5/Ru 5 (in nm). We confirmed from vibrating sample magnetometer and magneto-resistive (MR) curve measurements that the magnetic coupling of CoFeB and CoFeSiB is weak ferromagnetic coupling, although the mechanism of this coupling is not yet clear. Because of this magnetic coupling, the magnetization reversal process reflects that of the thick CoFeSiB layer with soft magnetic properties.[12] The coercive field ($\mu_0 H_c$) and magnetic anisotropy field ($\mu_0 H_k$) for 140 nm thick CoFeSiB layers are 0.01 and 0.10 mT, respectively. Thanks to these excellent soft magnetic properties of thick CoFeSiB layers, a maximum sensitivity of a single MTJ with 140 nm thick CoFeSiB was 1, 150%/mT that was 2.8 times larger than that for MTJs with 30 nm thick CoFeSiB.[12] For the preparation of very thin MgO barriers, the Mg layer of 0.7 nm was deposited on top of the bottom CoFeB layer and then oxidized by pure oxygen in the deposition chamber. To fully oxidize the Mg layer and obtain the intended thickness of the MgO barrier, the process of depositing 0.1 nm thick Mg layers and in situ natural oxidization was repeated several times in sequence.[15] The prepared MTJ multilayer films were microfabricated into MTJ arrays by photolithography and Ar ion milling. The TMR sensor has a structure in which 74 MTJs with device area of 50×50 μm^2 are

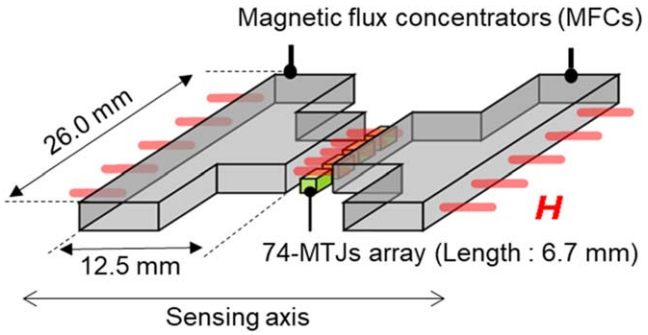

Fig. 1. (Color online) Schematic image of the developed TMR sensor with magnetic flux concentrators (MFCs).

connected in series to reduce the 1/*f* noise,[16–18] and the length of the 74-MTJ array is 6.7 mm. After the microfabrication, the MTJ arrays were annealed using the double annealing process with a magnetic field of 0.3 T to realize a linear output response against the external magnetic field.[11] The first and second annealing temperatures were 330 and 225 °C, respectively. The output of the TMR sensor dominantly changes with a magnetic field applied in the short-side direction (sensing axis) of the MTJ array. On both sides of the MTJ arrays, T-shaped MFCs, which are effective for concentrating the external magnetic field,[19,20] were prepared as shown in Fig. 1. Firstly, the MFCs of about 1 μm thick $Fe_{73.5}Cu_{1.0}Nb_{3.0}Si_{15.5}B_{7.0}$ films were deposited, and 0.5 mm thick $Ni_{80}Fe_{20}$ plates with T-shape were subsequently placed on the $Fe_{73.5}Cu_{1.0}Nb_{3.0}Si_{15.5}B_{7.0}$ films. The T-shaped MFCs have a size of 12.5 mm in the direction of the sensing axis (vertical line of "T") and 26.0 mm in the direction parallel to the MTJ array (horizontal line of "T"). We confirmed that the sensitivity with applying the magnetic field in the direction rotated 90 degrees in-plane from the sensing axis was negligible, because it was less than 1/10 of the sensitivity for the sensing axis.

Figure 2(a) shows TMR ratio dependence on the resistance area product (*RA*) for fabricated TMR sensors. *RA* values were controlled by varying repeat number of the Mg oxidation process from 13 to 20 times. The maximum TMR ratio of 195% at room temperature was obtained for TMR sensors with high *RA* value and the TMR ratio slightly decreased with decreasing *RA*, although the single MTJ device exhibited a larger TMR ratio, above 200%, and did not show marked *RA* dependence of TMR ratio. The observed degradation of the TMR ratio is due to the parasitic resistance from bottom electrodes to form 74-MTJ arrays and the effect of this parasitic resistance becomes remarkable as the device resistance decreases. Although the TMR ratio slightly decreased for the MTJ arrays with low *RA*, the voltage sensitivity was 1.8 times improved compared to previous work[14] from 0.45 to 0.83 μV nT^{-1} at 1 V utilizing a thick CoFeSiB layer with ultra-soft magnetic properties. Figure 2(b) shows the *RA* dependence of the detectivity at 1 Hz for developed TMR sensors. The detectivity improved as the *RA* decreased, despite the deterioration of the TMR ratio. The minimum detectivity of 0.94 pT/Hz$^{1/2}$ at 1 Hz was achieved in the TMR sensor with low *RA* value. This improvement in detectivity is considered to be due to the enhancement of sensitivity and reduction in the white noise because of decrease in device resistance. In addition, the reduction of electrical 1/*f* noise due to the decrease in the repeat number of the Mg oxidation process is also one of the reasons for the detectivity improvement. The evaluated electrical Hooge's parameter measured in parallel magnetization state, which indicates the magnitude of the electrical 1/*f* noise, was 6.0×10^{-9} um^2 ($RA = 4.1 \times 10^4$ Ω μm^2) and 1.2×10^{-9} um^2 ($RA = 1.5 \times 10^3$ Ω μm^2) for prepared MTJs. Since one of the origins of the electrical 1/*f* noise is hopping tunneling through the defects in the MgO barriers,[21] the repetition of the Mg oxidation process can increase the number of hopping states in the MgO barriers and the electrical 1/*f* noise. Since the electric Hooge's parameter for MTJs with MgO layers prepared by the RF sputtering technique is about one order of magnitude smaller,[22,23] further optimizations of the condition for Mg oxidation process are needed. However, the obtained small detectivity is about 1/100 of those for reported MR sensors,[14,18,19,24–26]

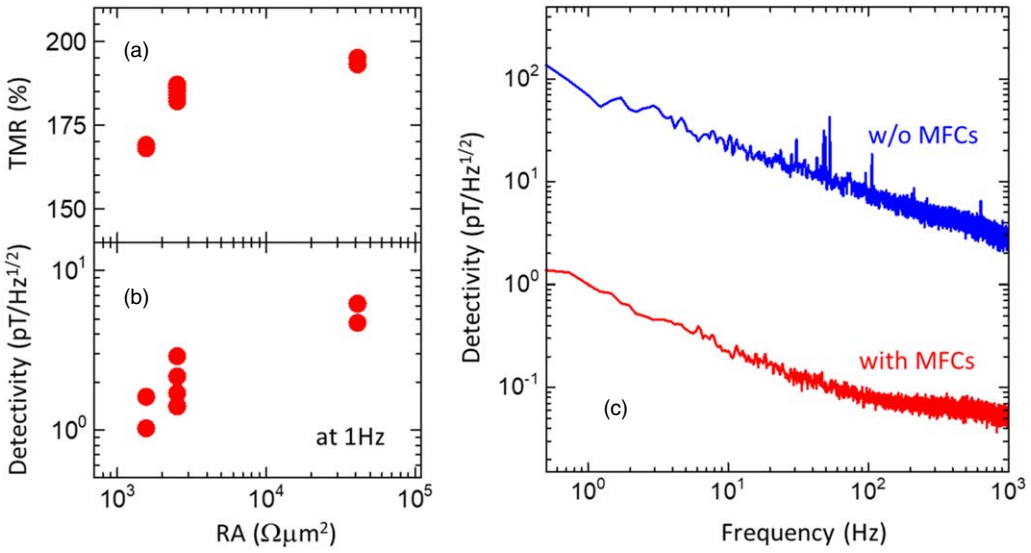

Fig. 2. (Color online) Resistance area products (*RA*) dependences of (a) TMR ratio and (b) detectivity in TMR sensors. (c) Detectivity spectrum for the TMR sensor with low *RA*.

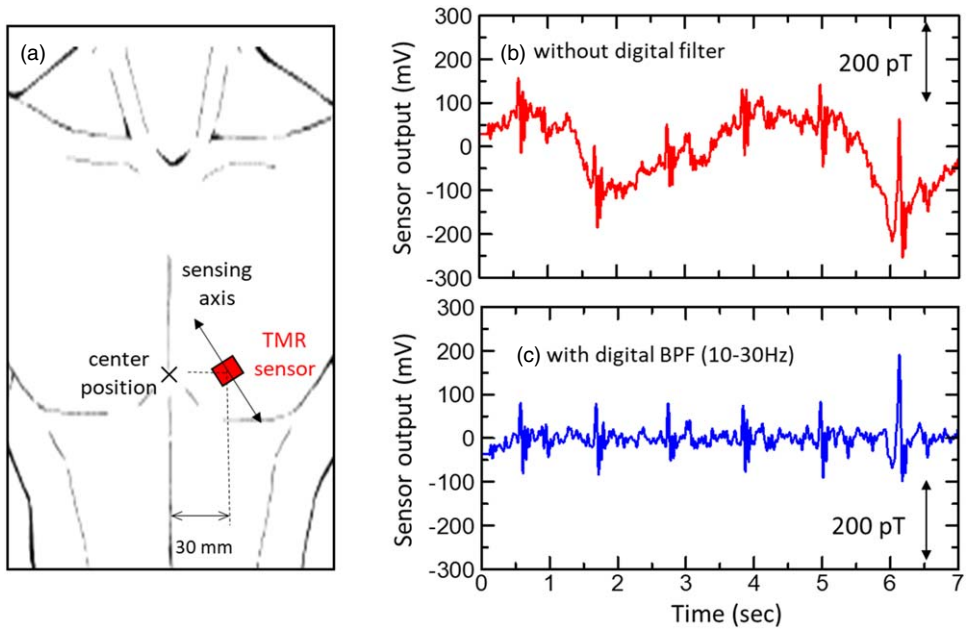

Fig. 3. (Color online) (a) Measurement position and sensing direction for MCG measurement using a TMR sensor. Real-time MCG measurement results obtained (b) without and (c) with a digital bandpass filter (10–30 Hz).

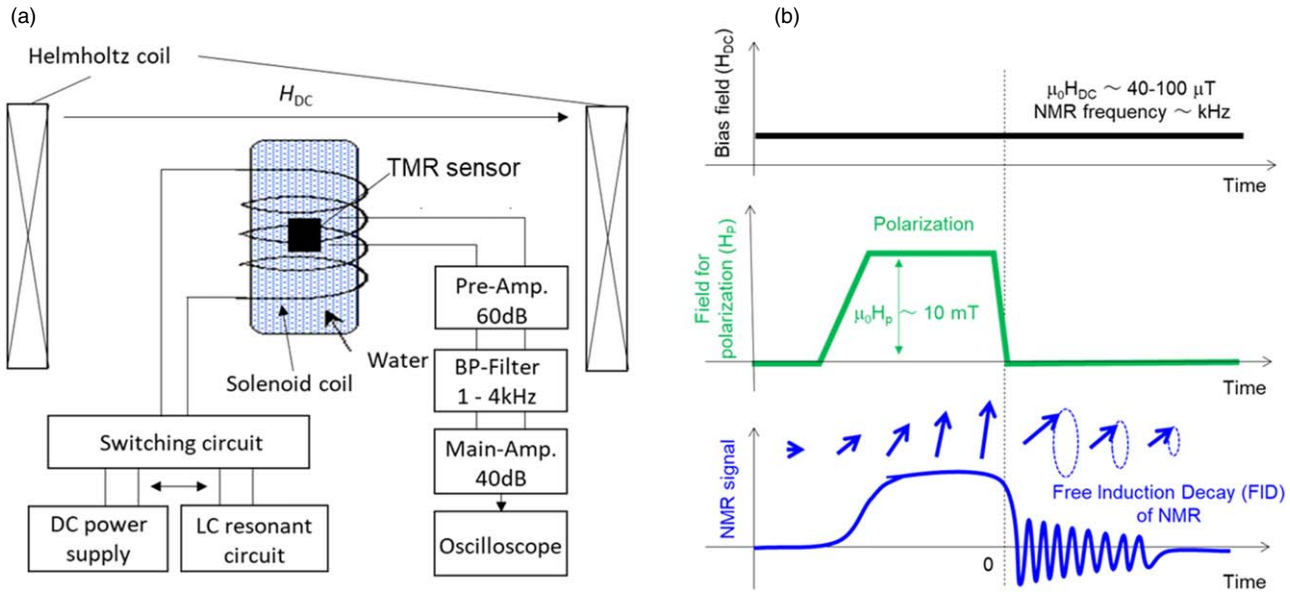

Fig. 4. (Color online) NMR measurement (a) system and (b) process flow using a TMR sensor.

and the other highly sensitive magnetic sensor devices, such as magneto-impedance (MI) sensors, flux-gate sensors, and diamond quantum sensors, have not yet realized such a small detectivity in the low frequency range.[27–29] Figure 2(c) shows the frequency dependence of the detectivity for the most sensitive TMR sensors with and without MFCs. For both sensors, a clear 1/*f* noise was observed and the corner frequency in the TMR sensor with MFCs was around 100 Hz. As shown in Fig. 2(c), the gain of MFCs was about 70 at 1 Hz, 87 at 10 Hz, and 44 at 1 kHz. A very small detectivity of 0.05 pT/Hz$^{1/2}$ (50 fT/Hz$^{1/2}$) at 1 kHz was achieved by attaching MFCs. The typical detectivity for SQUID sensors is 100 fT/Hz at 1 Hz and 10 fT/Hz at 1 kHz.[30] Although the achieved detectivity for developed TMR sensors is still 5–10 times larger than that for SQUID sensors, a feature of room temperature operation for TMR sensors is a great advantage and the obtained detectivity is enough to measure MCG and NMR signals in real-time.

MCG measurements were carried out using the developed TMR sensors with the lowest detectivity. MCG is a clinical tool used to measure and localize electrical current in the heart, and it has been measured by SQUID sensors placed in Dewar vessels containing liquid helium.[31] However, Dewar wall thickness has been constituting a barrier to the minimization of sensor-source distance, the most important factor for spatial resolution of MCG. We fabricated an MCG measurement

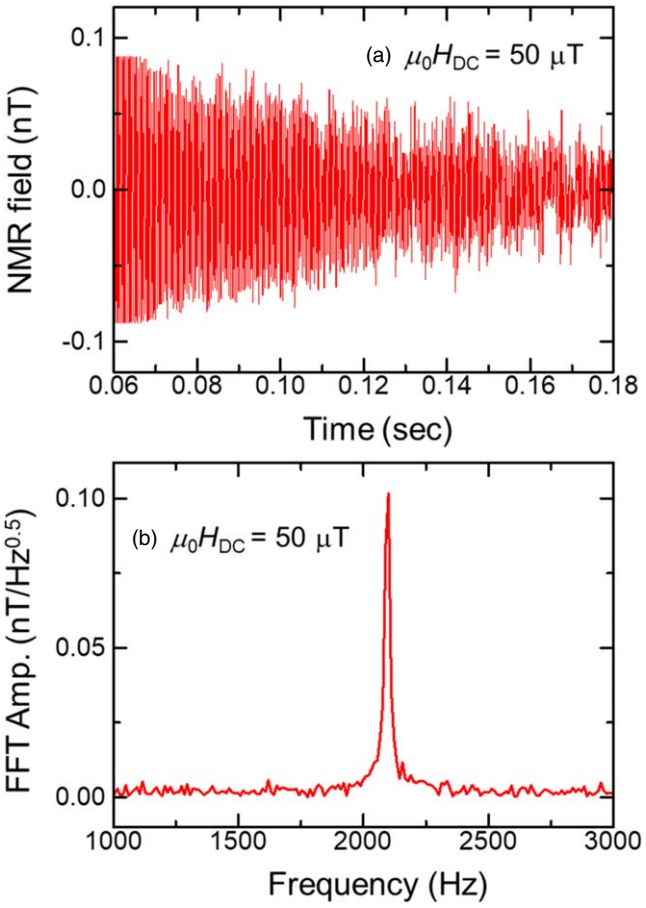

Fig. 5. (Color online) (a) Proton NMR signal and (b) the FFT spectrum measured by a TMR sensor.

module with TMR sensors that could be attached to the chest surface. For the MCG module, a TMR sensor was used as one of the resistors in the full-bridge circuit, and its output voltage was amplified and filtered. Bias voltage of ±0.2 V was supplied to the full-bridge circuit. The circuit to receive the signal from the bridge was constructed by ourselves using instrumentation amplifiers and capacitor-resistor (CR) passive filters. MCG signals measured by the TMR sensor bridge were input to a two-stage amplification circuit with a total gain of 100 dB and were shaped by an analog bandpass filter from 0.1 to 50 Hz. MCG measurements were performed on normal subjects (aged 26 years) in a magnetically shielded room. The MCG module was directly fixed on the anterior chest wall and the transverse component of MCG was measured at 30 mm to the left of the center of the chest as shown in Fig. 3(a). Figure 3(b) shows the typical result of real-time MCG measurement. Although the long-period signal was due to the body movement generated by respiration, the R-peaks of MCG were clearly observed. In order to eliminate signals due to body movements, the measured MCG signals were filtered in the software (digital filter) from 10 to 30 Hz. As shown in Fig. 3(c), we successfully recorded clear QRS components without signal averaging. The amplitude of the transverse magnetic field related to the R-peaks was approximately 100–200 pT, which is consistent with the reported value measured by SQUIDs.[31] However, we need about 10 times improvement in detectivity to clearly measure small peaks of MCG (P, Q, and T peaks) by real-time measurement. In order to detect these small MCG peaks, the reduction in the large electrical 1/*f* noise due to hopping states in the MgO barriers is required by optimizations of the Mg oxidation process.

We also performed proton NMR measurements under low magnetic field as another application of bio-magnetic field measurements. If the proton NMR signal can be detected under a low external magnetic field similar to the geomagnetism, TMR sensors are also expected to be applied to a compact magnetic resonance imaging (MRI) system in the future. Although low magnetic-field MRI systems using SQUIDs and optically pumped magnetometers have already been demonstrated,[32,33] they are not compact because the sensors do not operate at room temperature. On the other hand, TMR sensors have a great advantage of room temperature operation to realize a compact MRI system. As mentioned above, since the developed TMR sensors exhibit very small detectivity, below 0.1 pT/Hz$^{1/2}$ at the kHz frequency range, NMR signals with 1–4 kHz frequency under low external magnetic field can be measured. For the NMR measurements, the full-bridge circuit with a TMR sensor and three fixed resistors was developed, and the output voltage was input to an amplifier circuit. The total gain of the amplifier circuits was 100 dB, and the signal was passed through a bandpass filter with a range of 1–4 kHz. A solenoid coil for exciting proton nuclear magnetization was wound around a container containing 50 c.c. of water, and a TMR sensor was placed in the center of the container. In addition, a Helmholtz coil for applying an external magnetic field was set on the outside of the coiled container [Fig. 4(a)]. After exciting the nuclear magnetization by applying a pulse magnetic field of 10 mT with the solenoid coil, the relaxation process of the nuclear magnetization in the direction of the DC external magnetic field generated by the Helmholtz coil was measured by the TMR sensor [Fig. 4(b)]. Figure 5(a) shows a typical NMR signal caused by free-induction-decay (FID) motion of nuclear spins when the applied external magnetic field was approximately 50 μT. A clear FID signal was observed; the maximum amplitude of a nuclear magnetic field was about 100 pT and the transverse relaxation time (T_2) was about 120 msec. Figure 5(b) is the result of FFT of the NMR signal shown in Fig. 5(a). The peak frequency of 2.10 kHz is consistent with the expected resonance frequency of 2.13 kHz for proton nuclear magnetization under 50 μT.[34] Thus we succeeded in observing a clear NMR signal by real-time measurement using the developed TMR sensors.

In summary, we have succeeded in developing an ultra-sensitive TMR sensor that can detect sub-pT magnetic fields in the low frequency range. The achieved detectivity was 0.94 pT/Hz$^{1/2}$ at 1 Hz and 0.05 pT/Hz$^{1/2}$ at 1 kHz, which is the lowest value to date among magneto-resistive magnetic sensors. The extremely small detectivity of our TMR sensors is due to the low noise because of the reduction in *RA* for the MTJs and to the high output obtained by using both thick CoFeSiB layers with excellent soft magnetic properties and MFCs. In addition, by using the developed TMR sensors, we observed clear MCG signals in real-time and succeeded in detecting the NMR signal of protons for the first time. These results indicate that both MCG and MRI can be measured by the same measurement system with TMR sensors. We believe the result will open a door into new applications of MCG and MRI for both basic and medical sciences.

Acknowledgments This work was supported by the Center for Science and Innovation in Spintronics (CSIS), the Center for Innovative Integrated Electronic System (CIES), the Center for Spintronics Research Network (CSRN), and the S-Innovation program, Japan Science and Technology Agency (JST).

ORCID iDs Takafumi Nakano https://orcid.org/0000-0002-9451-0014 Shigemi Mizukami https://orcid.org/0000-0001-9913-1833

1) W. H. Butler, X.-G. Zhang, T. C. Schulthess, and J. M. MacLaren, Phys. Rev. B **63**, 054416 (2001).
2) J. Mathon and A. Umerski, Phys. Rev. B **63**, 220403 (2001).
3) S. Yuasa, A. Fukushima, T. Nagahama, K. Ando, and Y. Suzuki, Jpn. J. Appl. Phys. **43**, L588 (2004).
4) S. Yuasa, T. Nagahama, A. Fukushima, Y. Suzuki, and K. Ando, Nat. Mater. **3**, 868 (2004).
5) S. S. P. Parkin, C. Kaiser, A. Panchula, P. M. Rice, B. Hughes, M. Samant, and S. Yang, Nat. Mater. **3**, 862 (2004).
6) D. D. Djayaprawira, K. Tsunekawa, M. Nagai, H. Maehara, S. Yamagata, N. Watanabe, S. Yuasa, Y. Suzuki, and K. Ando, Appl. Phys. Lett. **86**, 092502 (2005).
7) S. Ikeda, J. Hayakawa, Y. Ashizawa, Y. M. Lee, K. Miura, H. Hasegawa, M. Tsunoda, F. Matsukura, and H. Ohno, Appl. Phys. Lett. **93**, 082508 (2008).
8) S. Ikegawa, F. B. Mancoff, J. Janesky, and S. Aggarwal, IEEE Trans. Electron Devices **67**, 1407 (2020).
9) H. Yoda et al., Curr. Appl Phys. **10**, e87 (2010).
10) S. Mao et al., IEEE Trans. Magn. **42**, 97 (2006).
11) K. Fujiwara, M. Oogane, S. Yokota, T. Nishikawa, H. Naganuma, and Y. Ando, J. Appl. Phys. **111**, 07C710 (2012).
12) D. Kato, M. Oogane, K. Fujiwara, T. Nishikawa, H. Naganuma, and Y. Ando, Appl. Phys. Express **6**, 103004 (2013).
13) K. Ishikawa, M. Oogane, K. Fujiwara, J. Jono, M. Tsuchida, and Y. Ando, Jpn. J. Appl. Phys. **55**, 123001 (2016).
14) K. Fujiwara et al., Appl. Phys. Express **11**, 023001 (2018).
15) X. Chen and P. Freitas, Nano-Micro Lett. **4**, 25 (2012).
16) M. Tondra, J. M. Daughton, D. Wang, R. S. Beech, A. Fink, and J. A. Taylor, J. Appl. Phys. **83**, 6688 (1998).
17) K. Fujiwara, M. Oogane, T. Nishikawa, H. Naganuma, and Y. Ando, Jpn. J. Appl. Phys. **52**, 04CM07 (2013).
18) J. G. Deak, Z. Zhou, and W. Shen, AIP Adv. **7**, 056676 (2017).
19) G. He, Y. Zhang, L. Qian, G. Xiao, Q. Zhang, J. C. Santamarina, T. W. Patzek, and X. Zhang, Appl. Phys. Lett. **113**, 242401 (2018).
20) X. Zhang, Y. Bi, G. Chen, J. Liu, J. Li, K. Feng, C. Lv, and W. Wang, AIP Adv. **8**, 125222 (2018).
21) A. Gokcea, E. R. Nowak, S. H. Yang, and S. S. P. Parkin, J. Appl. Phys. **99**, 08A906 (2006).
22) R. Stearrett, W. G. Wang, L. R. Shah, A. Gokce, J. Q. Xiao, and E. R. Nowak, J. Appl. Phys. **107**, 064502 (2010).
23) J. M. Almeida, P. Wisniowski, and P. P. Freitas, IEEE Trans. Magn. **44**, 2569 (2008).
24) A. V. Silva, D. C. Leitao, J. Valadeiro, J. Amaral, P. P. Freitas, and S. Cardoso, Eur. Phys. J. Appl. Phys. **72**, 10601 (2015).
25) S. Cardoso, D. C. Leitao, L. Gameiro, F. Cardoso, R. Ferreira, E. Paz, and P. P. Freitas, Microsyst. Technol. **20**, 793 (2014).
26) R. Ferreira, E. Paz, P. P. Freitas, J. Wang, and S. Xue, IEEE Trans. Magn. **48**, 3719 (2012).
27) T. Uchiyama and J. Ma, IEEE Trans. Magn. **55**, 4400408 (2019).
28) C. C. Lu and J. Huang, Sensors **15**, 14727 (2015).
29) E. D. Herbschleb, H. Kato, T. Makino, S. Yamasaki, and N. Mizuochi, Nat. Commun. **12**, 306 (2021).
30) J. Kawai, M. Miyamoto, M. Kawabata, and G. Uehara, IEEE Trans. Appl. Supercond. **28**, 1602607 (2018).
31) H. Koch, IEEE Trans. Appl. Supercond. **11**, 49 (2001).
32) P. T. Vesanen et al., Magn. Reson. Med. **69**, 1795 (2013).
33) I. Hilschenz, Y. Ito, H. Natsukawa, T. Oida, T. Yamamoto, and T. Kobayashi, J. Magn. Reson. **274**, 89 (2017).
34) F. Bloch, W. W. Hansen, and M. Packard, Phys. Rev. **70**, 474 (1946).